

1 **Mathematical and experimental evaluation of a mini-channel PV/T and thermal**
2 **panel in summer mode**

3 Jinzhi Zhou^{b, a}, Xudong Zhao^{c, a, *}, Yanping Yuan^b, Yi Fan^a, Jing Li^a

4 ^aSchool of Engineering and Computer Science, University of Hull, Hull, UK

5 ^bSchool of Mechanical Engineering, Southwest Jiaotong University, Chengdu, China

6 ^cDepartment of Power Engineering, North China Electric and Power Engineering,
7 Baoding, China

8 **Corresponding email: Xudong.Zhao@hull.ac.uk*

9 **Abstract:** In this paper, a mini-channel PV/T and mini-channel thermal panel hot water
10 system is presented. The thermal panels in this system use mini-channel tube as the heat
11 exchanger, which has a small hydraulic diameter and large heat exchanger area, and
12 this special structure can improve the heat transfer coefficient at the same flow rate than
13 the conventional type. The performance of this system for generating hot water and
14 electricity in summer has been tested, and a simulation model of this operating mode
15 has been developed. Based on a typical day's weather data, the simulation model is
16 verified, and the experimental and simulated results agree with each other very well.
17 The results reveal that the experimental and simulated electrical efficiencies of PV/T
18 panels are 11.5% and 12.6%, respectively. The experimental and simulated thermal
19 efficiencies of thermal collectors are 46.8% and 48.0%, respectively. The experimental
20 and simulated final water temperatures in the tank are 59.3 °C and 60.9 °C, respectively.
21 Based on these results, an error analysis is carried out. The experimental and simulation
22 results of the system in summer provide a fundamental data and method for predicting

23 the annual performance of the system in the future.

24 **Keywords:** Mini-channel, PV/T, thermal collector, hot water, efficiency

25 NOMENCLATURE

26 A Area, m^2

27 C_p Specific heat at constant pressure, $Jkg^{-1}K^{-1}$

28 D Hydraulic diameter,

29 d Thickness, m

30 E_{pv} Power output of PV layer, Wm^{-2}

31 G Solar radiation, Wm^{-2}

32 k Thermal conductivity, $Wm^{-1}K^{-1}$

33 l Thickness of the air gap, m

34 M_w Quality of water in the tank, kg

35 \dot{m}_{wf} Mass flow rate of working fluid, $kg s^{-1}$

36 Nu Nusselt number,

37 Pr Prandtl number,

38 R Thermal resistance, KW^{-1}

39 Ra Rayleigh number,

40 Re Reynolds number,

41	T	Temperature, K
42	U	Heat transfer co-efficient, $\text{Wm}^{-2}\text{K}^{-1}$
43	u_{wd}	Wind speed, ms^{-1}
44	α	Absorptivity,
45	β	Angle of inclination of the plane with the horizontal,
46	σ	Stefan-Boltzmann's constant,
47	τ_g	Glass transmissivity,
48	ε	Emissivity,
49	η	Efficiency,
50	ρ	Density, kg/m^3

51 ***Subscripts***

52	air	Air,
53	am	Ambient,
54	am_{gc}	Glass cover and ambient,
55	b	Absorber plate,
56	b_{am}	Absorber plate and ambient,
57	p_b	Absorber plate and mini-channel tube,
58	b_{gc}	Absorber plate and glass cover,

59	<i>e</i>	Electricity,
60	<i>gc</i>	Glass cover,
61	<i>hcg</i>	Heat-conducting glue,
62	<i>pv_gc</i>	Glass cover and PV layer,
63	<i>mc</i>	Mini-channel tube,
64	<i>Pwf</i>	Mini-channel tube and working fluid,
65	<i>pv</i>	PV layer,
66	<i>b_pv</i>	PV layer and absorber plate,
67	<i>pvt</i>	PV/T panel,
68	<i>rc</i>	Standard condition,
69	<i>s</i>	Sky,
70	<i>tk</i>	Storage tank,
71	<i>tk.i</i>	Inlet of storage tank,
72	<i>tk.o</i>	Outlet of storage tank,
73	<i>t.th</i>	Thermal energy of thermal collector,
74	<i>th</i>	Thermal collector,
75	<i>th.i</i>	Inlet of thermal collector,
76	<i>th.o</i>	Outlet of thermal collector,

77 *w* Water,

78 *wd* Wind,

79 *wf* Working fluid,

80 **1. Introduction**

81 Global energy consumption has increased steadily in past years (Tzeiranaki et al., 2018;
82 Bertoldi et al., 2013). The high living level, i.e., lighting, cooling and heating, has
83 translated to increase in the energy consumption of building. In 2016, the residential
84 energy consumption accounted for 25.71% of the EU's final energy consumption
85 (Tzeiranaki et al., 2013). In China, it accounted for 20.6% of the total energy
86 consumption (China Building Energy Research Report 2018). For the energy
87 consumption in building, space heating and hot water takes the largest share, using 78%
88 and 15% of the total residential energy usage in EU (EUROPEAN COMMISSION
89 2016), and space heating and hot water supply contribute 68% of energy consumption
90 in China (Zheng et al., 2014). Therefore, it is very important to develop renewable
91 energy system to replace the fossil energy consumption for reducing CO₂ emission and
92 improving the environment.

93 Solar energy is a type of green and free renewable energy, which can be collected by
94 PV panel, thermal collector and PV/T panel. These panels can be integrated to the
95 building easily, therefore, it is a good way to combine solar energy panels to building
96 for supplying electricity and thermal energy. Thermal collector is the most investigated

97 technology to translate solar energy into thermal energy for generating hot water
98 (Goswami et al., 2015). It can be cooled by air (Khanlari et al., 2020; Ural et al., 2019),
99 water (Araya et al., 2017; Hajabdollahi et al., 2017), nanofluid (Eltaweel et al., 2019;
100 Noghrehabadi et al., 2016), heat pipe (Zhang et al., 2017; Allouhi et al., 2019) and
101 refrigerant (Aziz et al., 1999; Sun et al., 2014). K. Balaji et al. (Balaji et al., 2017)
102 constructed a solar collector hot water system using heat transfer enhancer in absorber
103 tube. It was found that the rod heat transfer enhancer provides higher heat transfer with
104 a small increase in pumping power than tube heat transfer enhancer and plain tube flat
105 plate solar collector. Edalatpour et al. (Edalatpour et al., 2017) investigated the thermal-
106 hydraulic characteristics and exergy performance of tube-on-sheet flat plate solar
107 collector using different working fluid. Col et al. (Col et al., 2013) compared the thermal
108 performance of flat plate solar collectors with sheet-and-tube and roll-bond absorbers,
109 and the result revealed that the roll-bond absorber has a much higher thermal efficiency.

110 PV/T is a device which combines PV panel and thermal collector together, and it can
111 provide power and thermal energy at the same time (Kaushik et al., 2012; Joshi et al.,
112 2018). It is an improved product based on PV panel and thermal collector, therefore,
113 the coolant is the same as the thermal collector (Sarhaddi et al., 2010; Chow et al., 2007;
114 Sardarabadi et al., 2017; Pei et al., 2011; Zhou et al., 2016). Zondag et al. (Zondag et
115 al., 2003) experimentally investigated a sheet and tube PVT collector, and the result
116 indicated that its daily thermal and electrical efficiency were 58% and 8.9%. Pang et al.
117 (Pang et al., 2019) experimentally and theoretically studied a roll-bond PV/T hot water

118 system, and the daily electrical, thermal and exergy efficiency of the PVT system were
119 13.67%, 40.56% and 15.56%. Chow et al. (Chow et al., 2006) tested a flat-box PV/T
120 hot water system, and the results revealed that the electrical efficiency ranged from 10.7%
121 to 12.3%, and thermal efficiency ranged from 39.0% to 48.6%.

122 Currently, both the PV/T panel and thermal collector use copper tube or flat-box as the
123 heat exchanger to transfer solar energy. These tubes have a big cross section and
124 hydraulic diameter, which decreases the Reynolds number and heat exchanger co-
125 efficient of working fluid. To improve the heat transfer rate and overall efficiency of
126 PV/T panel and thermal collector, mini-channel tube is chosen to replace the
127 conventional heat exchanger. Mini-channel tube is a new type of heat exchanger, and it
128 has a small hydraulic diameter ($1\text{mm} < D_h < 6\text{mm}$) (Dixit et al., 2015). The reduced
129 equivalent diameter of the micro-channel can enhance its heat transfer rate under the
130 same flow rate (Prajapati et al., 2016; Khan et al., 2014). In addition, the smooth surface
131 of mini-channel tube has a bigger contact area with the absorber than copper tube.

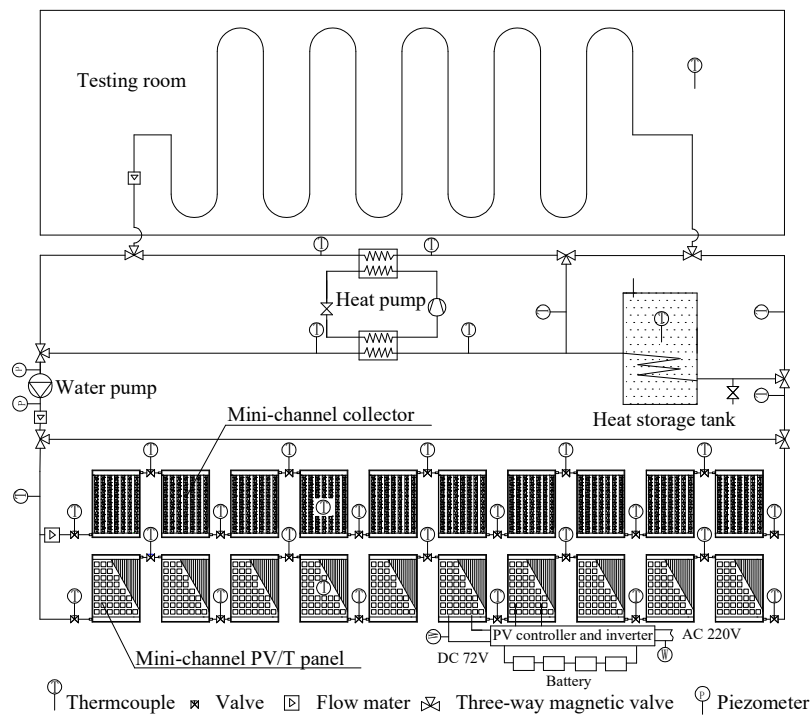
132 Based on the benefit of mini-channel heat exchanger, a mini-channel PV/T panels and
133 thermal collectors combined heat pump system is designed and constructed, which can
134 provide thermal energy for space heating, generate electricity and hot water with a much
135 higher energy efficiency. In this paper, the performance of this system in summer is
136 tested for generating electricity and hot water. With the experimental data as the input
137 parameters, a simulation model is developed and verified.

138

139 **2. System setup**

140 **2.1 System description**

141 As shown in Fig. 1, each of the 10 mini-channel PV/T panels and thermal collectors are
142 connected in series, and then these two types of panels are connected in parallel, which
143 can provide thermal energy and electricity for building. The testing room and water
144 storage tank are connected in parallel and then linked to the solar panels system, which
145 can consume and store thermal energy from solar panels. A water heat pump is set
146 between the water storage and testing room, which can transfer thermal energy from
147 storage tank to testing room in the night. For meeting different requirement of building
148 in different seasons, this system has two operating modes, which are presented as
149 follows:



151 **Fig. 1 Mini-channel PV/T panels and thermal collectors combined heat pump**
152 **system (Zhou et al., 2017)**

153 **Space heating mode:** In winter, when the system starts, the working fluid goes
154 thorough mini-channel PV/T panels and thermal collector. If the solar radiation is weak
155 and the thermal energy generated by the solar panels is not enough for space heating,
156 the working fluid only enters the heat exchanger inside of the tank and releases energy
157 to water. With the increase of solar radiation, if the temperature of working fluid at
158 outlet of solar panels is higher than 40 °C, the working fluid goes through storage tank
159 and testing room at the same time. One part is for space heating, and the other is for
160 storing surplus energy. In the night, the heat pump system starts and absorbs energy
161 from storage tank and releases energy to testing room for space heating continually.

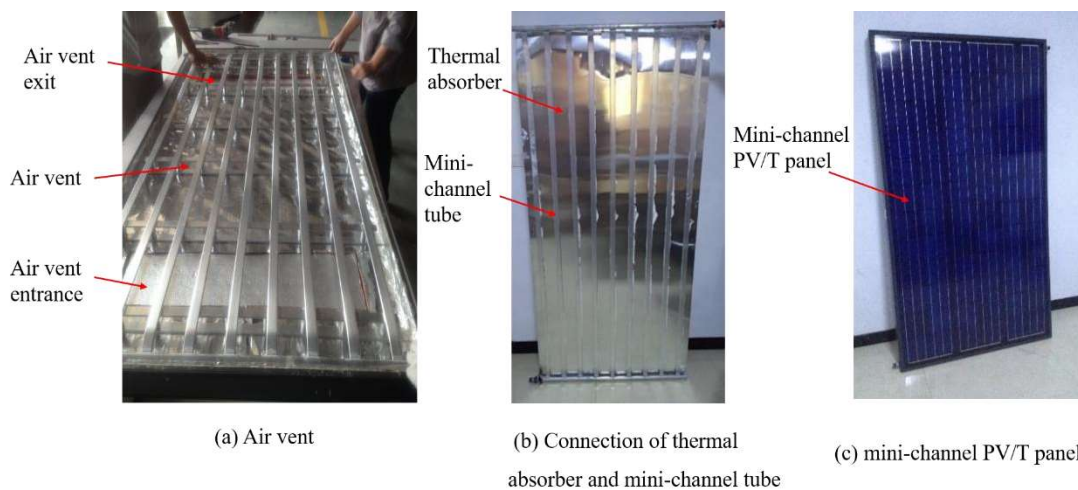
162 **Hot water mode:** In other seasons, this system can generate hot water and electricity
163 for building. The working fluid goes through thermal collectors where it is heated, and
164 then enters the heat exchanger inside of storage tank where the heat exchange takes
165 place, releasing energy to water. The cooled working fluid goes back and enters thermal
166 collectors again, completing a circulation. The air-vent at the back of mini-channel
167 PV/T panel opens, and the air goes through it and cools the PV cell naturally.

168 **2.2 System components**

169 **Mini-channel PV/T**

170 To improve the annual electricity output, mini-channel PV/T panel is designed to be an

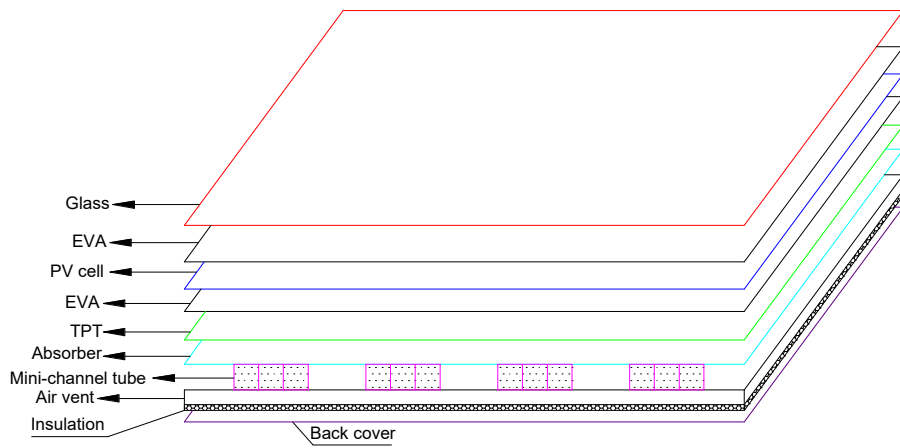
171 unglazed type (**Fig. 2**) which consist a standard PV panel and a mini-channel layer. The
172 constituent layers of this PVT collector are shown in **Fig. 3**. The size of PV/T panel is
173 $1000 \text{ mm} \times 2000 \text{ mm}$. 72 pieces of polycrystalline silicon PV cells (size $156 \text{ mm} \times 156$
174 mm) are connected in series and laminated on the glass. Its working voltage is 36 V,
175 and maximum output power is 310 W, and electrical efficiency is 18% under standard
176 condition. The mini-channel layer is composed of a piece of aluminium plate (size 1950
177 $\times 950 \times 0.4 \text{ mm}$) and mini-channel heat exchanger, which are connected by thermally
178 conductive glue. As shown in **Fig. 4**, nine mini-channel tube (**Fig. 5**) are welded into
179 the two header pipes in parallel, and each of the header pipes is composed of two blind
180 pipes, which work together to separate the nine mini-channel tubes to be three parts.
181 An air vent is designed between the insulation and absorber plate, which can cool down
182 the PV cell naturally in summer.



183

184

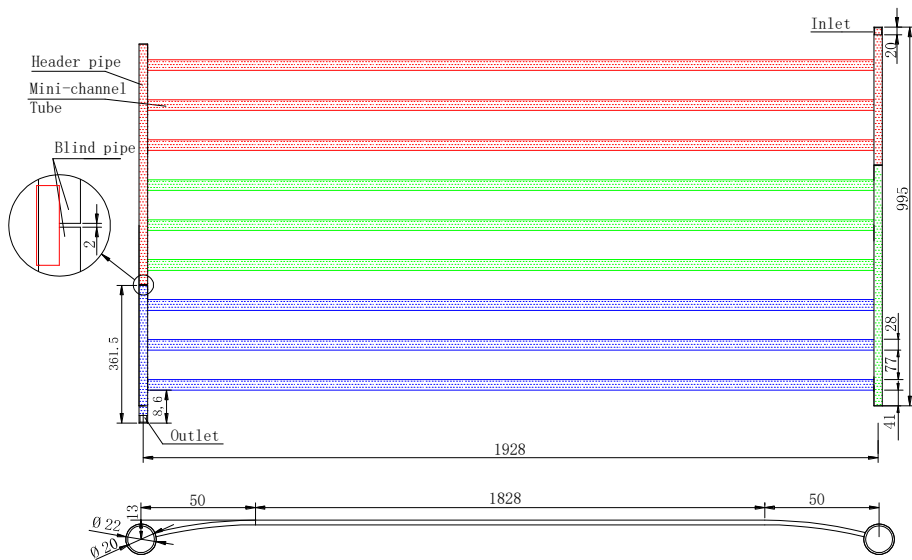
Fig. 2 Mini-channel PV/T panel



185

Fig. 3 Constituent layers of mini-channel PVT collector

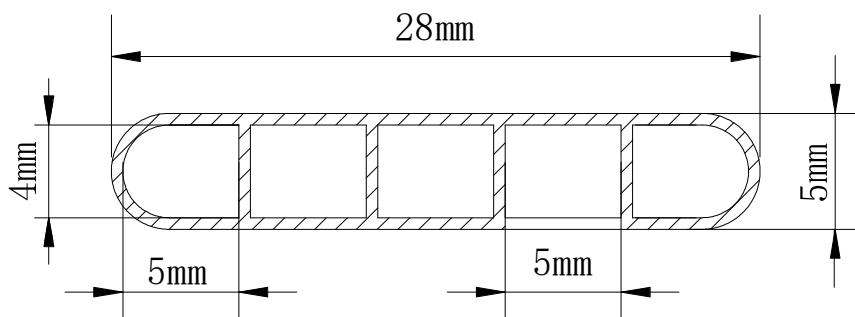
186



187

Fig. 4 Drawing of mini-channel layer

188



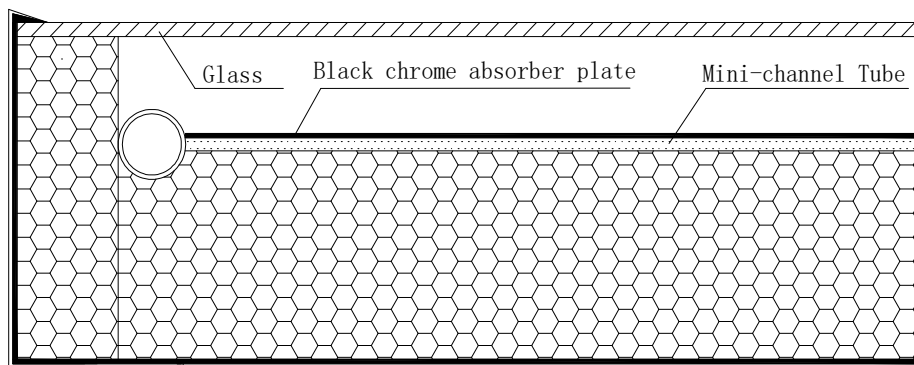
189

Fig. 5 Drawing of mini-channel tube

190

191 **Mini-channel thermal collector**

192 To improve the thermal energy generation, Mini-channel thermal collector is designed
193 to be a glazed type, which has a similar structure as the PV/T panel, and the difference
194 between them are that: 1) an air gap is designed between the glass cover and absorber;
195 2) PV cells are removed; 3) an absorber with black chrome replacing the aluminium
196 plate in PV/T panel; 4) air vent is removed. Tts structure is shown in **Fig. 6 and Fig. 7.**



197

198 **Fig. 6 Sectional view of the mini-channel solar thermal panel**



199

200 **Fig. 7 Mini-channel solar thermal panel**

201 The sizes and material of each component is shown in **Table 1.** Several parameters in
202 this system, i.e. temperature, flow rate, power output, current, etc., are tested and

203 collected, and the technical properties of the measurement devices are given in **Table 2**
 204 **(Zhou et al. 2017)**.

205 **Table 1 Sizes and description of the components**

NO	Components	Size	Description
1	PV/T	2000*1000*80 mm	Effective area:1.85 m ² Maximum output power : 310 W Electrical efficiency: 17%
2	Thermal panel	2000*1000*80 mm	Effective area:1.85m ²
3	Heat storage tank	1 m ³	Height:1180 mm Diameter:1190 mm Thickness of insulation: 50 mm
4	Coil-type-heat-exchanger	1.32 m ²	Quantity: 2 Diameter:15 mm Thickness:1 mm Length:14 m
5	Heat pump	880*660*1470 mm	Refrigerant: R-22 Cooling capacity: 9.9 KW Input power: 2.1 KW Heating capacity: 12 KW
6	Inverter	400*850*850 mm	Output power: 4 kW Input direct voltage: 24 V Output alternating voltage: 220 V
7	Water pump	12.6 kg	Max.lift head: 25 m Max Input power: 850 W Max flow rate: 115L/min

206 **Table 2 Technical properties and uncertainties of the measurement devices**

Devices	Specification	Property	Sensibility	Uncertainty	Location
Power sensor	HK-D4I CE- P03-32BS	0~2200 W	1%	±11W	In the room, Connected to the heat pump
Pyranometer	TQB-2	0~2000 W/m ²	7~14μV/Wm ⁻²	< ±2%	Top of panel
Water flowmeter	LWGY-C	0.5~10 m ³ /h	-	±1%	Entrance of PV/T and thermal panels, exit of room, Entrance of PV/T

Current sensor	HK-14	0~10 A	±1%	-	In the room, connected to the PV/T panel
Thermocouple	T type	-200~+350 °C	±0.5 °C	±0.5 °C±0.1%*T	absorber of PV/T and thermal panel, Entrance and exit of PV/T, thermal panel, storage tank, testing room, evaporator and condenser of heat pump, ambient and room temperature.
Data logger	34970 A	20 channel	-	-	In the room
Pressure gauge	YN60	0-600 kpa	±1%	±6 kpa	Entrance and exit of water pump

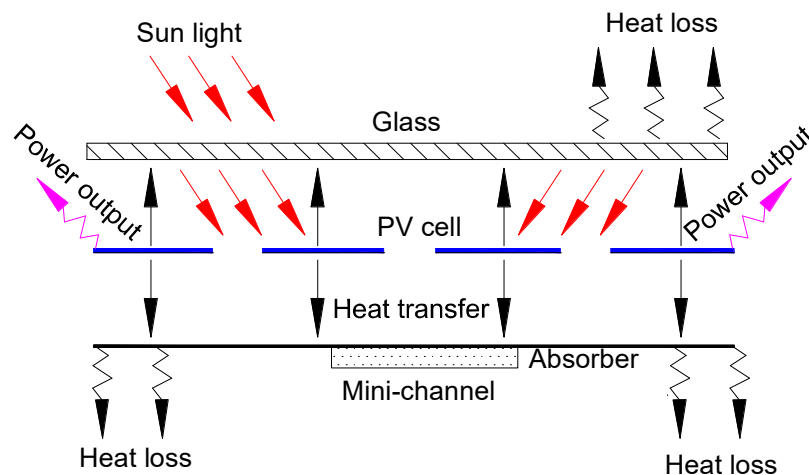
207

208 3. Simulation model

209 3.1 Simulation model for mini-channel PV/T panel

210 The simulation model of mini-channel PV/T panel consists of glass cover, PV layer,
 211 absorber and mini-channel heat exchanger. And the heat transfer process is shown in

212 **Fig. 8.**



213

214 **Fig. 8 Energy transfer process in mini-channel PV/T panel**

215 For glass cover (Chow et al., 2006)

$$216 \quad d_{gc} \rho_{gc} C_{p,gc} \frac{\partial T_{gc}}{\partial t} = G \lambda_{gc} + \alpha_{pv_gc} (T_{gc} - T_{pv}) - \alpha_{am_gc} (T_{gc} - T_{am}) \quad (1)$$

$$217 \quad \alpha_{am_gc} = 2.8 + 3.0 u_{wd} \quad (2)$$

218 where, d_{gc} is the thickness of the glass cover (m); ρ_{gc} is the density of glass cover
219 (kg/m^3); $C_{p,gc}$ is the specific heat capacity of glass cover ($\text{J}/(\text{kg}\cdot\text{K})$); T_{gc} is the
220 temperature of the glass cover (K); T_{am} is the ambient temperature (K); α_{am_gc} and
221 α_{pv_gc} is the heat transfer co-efficient between the glass cover and the ambient air and
222 PV cell respectively ($\text{W}/(\text{m}^2\cdot\text{K})$); S_{wd} is the wind speed (m/s); u_{wd} is the wind speed
223 (ms^{-1}).

224 For PV layer (Chow et al., 2006)

$$225 \quad \zeta d_{pv} \rho_{pv} C_{p,pv} \frac{\partial T_{pv}}{\partial t} = G (\tau \alpha)_{pv} - \frac{T_{pv} - T_b}{R_{b_pv}} - \alpha_{pv_gc} (T_{pv} - T_{gc}) - E_{pv} \quad (3)$$

$$226 \quad E_{pv} = \alpha_{pv} \tau_g G A_{pv} \eta_{rc} [1 - 0.0045 (T_{pv} - T_{rc})] \quad (4)$$

227 Where, ζ is coverage factor of PV cell; d_{pv} is the thickness of the PV cell (m); ρ_{pv}
228 is the density of PV cell (kg/m^3); $C_{p,pv}$ is the specific heat capacity of PV cell
229 ($\text{J}/(\text{kg}\cdot\text{K})$); α_{pv} is PV absorptivity; τ_g is Glass transmissivity; T_b is the temperature
230 of absorber plate (K); R_{b_pv} is the thermal resistance between PV layer and aluminium
231 plate ($\text{K}\cdot\text{m}^2/\text{W}$). E_{pv} is the power output of PV layer (Wm^{-2}); η_{rc} is the electrical
232 efficiency of PV under standard condition (18%); T_{rc} is the reference operating
233 temperature (298.15 K).

234 For absorber plate (Chow et al., 2006)

$$235 \quad \rho_b c_{p,b} \frac{\partial T_b}{\partial t} = K_b \frac{\partial^2 T_b}{\partial y^2} + \frac{1}{d_b} \left[\frac{T_{am} - T_b}{R_{b_am}} + \frac{T_{pv} - T_b}{R_{b_pv}} \right] \quad (5)$$

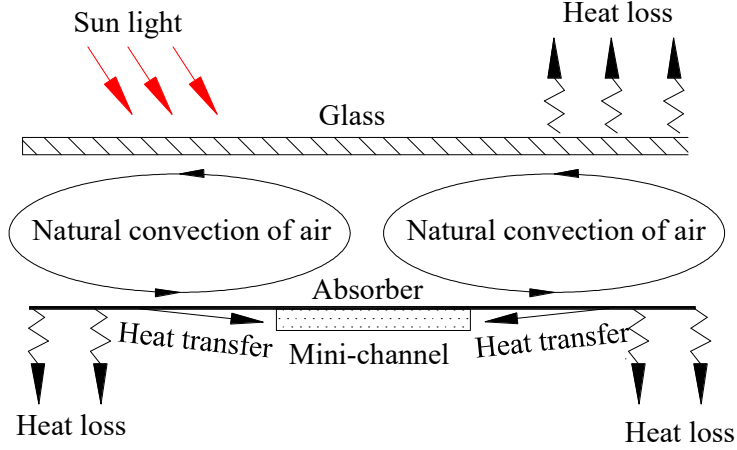
$$236 \quad R_{b_am} = \frac{l}{k_{air} Nu} \quad (6)$$

$$237 \quad Nu = 1 + 1.14 \left(1 - \frac{1708 \times (\sin 1.8\beta)^{1.6}}{Ra \times \cos \beta} \right) \left[1 - \frac{1708}{Ra \cos \beta} \right]^+ + \left[\left(\frac{Ra \times \cos \beta}{5830} \right)^{1/3} - 1 \right]^+ \quad (7)$$

238 Where, ρ_b , $C_{p,b}$, d_b , T_b and K_b are the density (kg/m^3), specific heat capacity
239 ($\text{J}/(\text{kg}\cdot\text{K})$), thickness (m), temperature (K) and thermal conductivity ($\text{W}/(\text{m}\cdot\text{K})$) of the
240 aluminium plate, respectively; R_{b_am} and R_{b_pv} is the thermal resistance between the
241 aluminium plate and surrounding, aluminium plate and PV layer (K/W). Nu is the
242 Nusselt number of the air between the insulation and absorber; β is the angle of
243 inclination of the plane with the horizontal; Ra is the Rayleigh number. + presents that
244 if the figure in the $[]^+ > 0$, then keep on, if not, the figure will be set at 0.

245 3.2 Mini-channel thermal collector

246 The simulation models of mini-channel thermal collector are composed of glass
247 cover, absorber plate, mini-channel heat exchanger and working fluid. They have a
248 similar energy transfer process and equations as the PV/T panel. The energy transfer
249 process is shown in **Fig. 9**, and the differences are as follows:



250

251

Fig. 9 Energy transfer process in mini-channel thermal panel

252 For glass cover (Chow et al., 2006)

253
$$d_{gc}\rho_{gc}c_{p,gc}\frac{\partial T_{gc}}{\partial t} = G\lambda_{gc} + \alpha_{b_{gc}}(T_{gc} - T_b) - \alpha_{am_{gc}}(T_{gc} - T_{am}) \quad (8)$$

254
$$\alpha_{b_{gc}} = \sigma(T_b^2 + T_{gc}^2)(T_b + T_{gc})\frac{1}{\frac{1}{\varepsilon_b} + \frac{1}{\varepsilon_{gc}} - 1} + \frac{Nu \cdot k_{air}}{l} \quad (9)$$

255 Where, $\alpha_{b_{gc}}$ is the heat transfer coefficient between the glass cover and absorber
 256 (W/(m²·K)); ε_b and ε_{gc} is the emissivity of the absorber and glass cover, respectively.

257 For absorber plate (Chow et al., 2006)

258 The absorber plate are divided into two parts: (1) the first part which connects the mini-
 259 channel directly; (2) the second part which acts as the fin. Their models are given as
 260 follows:

261 The equation of the first part can be expressed as:

262
$$\rho_b c_{p,b} \frac{\partial T_b}{\partial t} = K_b \frac{\partial^2 T_b}{\partial y^2} + \frac{1}{d_b} \left[G(\tau\alpha)_b - \frac{T_b - T_{am}}{R_{b_{am}}} - \frac{T_b - T_{gc}}{R_{b_{gc}}} - \frac{T_b - T_p}{R_{p_b A_{bi}}} \right] \quad (10)$$

263 The equation of the second part can be expressed as (Chow et al., 2006):

264
$$\rho_b c_{p,b} \frac{\partial T_b}{\partial t} = \lambda_b \frac{\partial^2 T_b}{\partial y^2} + \frac{1}{d_b} \left[G(\tau\alpha)_b - \frac{T_b - T_{am}}{R_{b_{am}}} - \frac{T_b - T_c}{R_{b_c}} \right] \quad (11)$$

265 Where, $(\tau\alpha)_b$ is the effective absorbance of the absorber plate. A_{bi} is the heat

266 exchange area of the selected microelement (m²), and its equation can be given as:

$$267 \quad A_{bi} = W_b \times dy \quad (12)$$

268 Where, W_b is the length of the panel (m); dy is the width of the selected
269 microelement (m).

$$270 \quad R_{p-b} = d_{hcg}/(K_{hcg}A_{p-b}) \quad (13)$$

271 Where, d_{hcg} and K_{hcg} are the thickness (m) and thermal conductivity (W/(m·K)) of
272 the heat-conducting glue, respectively; A_{p-b} is the contact area between the mini-
273 channel tube and aluminium plate (m²).

274 For mini-channel tube (Chow et al., 2006)

$$275 \quad \rho_p c_{p,p} \frac{\partial T_p}{\partial t} = K_p \frac{\partial^2 T_p}{\partial y^2} + \frac{1}{A_p} [\pi D_p \alpha_{pwf} (T_{wf} - T_p) + (T_b - T_p)/R_{p-b}] \quad (14)$$

$$276 \quad \alpha_{pwf} = 0.023 \frac{Re_{wf}^{0.8} Pr_{wf}^{0.3} k_{wf}}{D_p} \quad (15)$$

277 where, ρ_p , $C_{p,p}$ and K_b are the density (kg/m³), specific heat capacity (J/(kg·K)) and
278 thermal conductivity (W/(m·K)) of the micro-channel tube, respectively; A_p is the
279 cross section area of the micro-channel tube; D_p is the hydraulic diameter of mini-
280 channel (m); α_{pwf} is heat transfer co-efficient between mini-channel tube and
281 working fluid (Wm⁻²K⁻¹); T_{wf} is the temperature of working fluid (K);

282 For working fluid (Chow et al., 2006)

$$283 \quad (mc_p)_{wf} \frac{\partial T_{wf}}{\partial t} = (T_p - T_{wf})/R_{pwf} \quad (16)$$

284 where, m is mass flow of working fluid in one calculation unit (kg); R_{pwf} is the
285 thermal resistance between the micro-channel tube and working fluid (K/W).

286 3.3 Simulation model for water in the storage tank

287 The water in the tank is used for storing the thermal energy from the solar panels, and
288 its equation can be expressed as (Chow et al., 2006):

$$289 \quad M_w C_{p,w} \Delta T = \dot{m}_{wf} C_{p,wf} (T_{tk,i} - T_{tk,o}) + \alpha_{wam} A_{tk} (T_{am} - T_w) \quad (17)$$

290 where, M_w is the quality of water in the tank (kg); \dot{m}_{wf} is mass flow rate of working
291 fluid in the tank (kg s^{-1}); α_{wam} is the heat transfer co-efficient between water and
292 ambient ($\text{W m}^{-2} \text{K}^{-1}$); A_{tk} is the outside surface of tank (m^2); $T_{tk,i}$, $T_{tk,o}$ and T_w are
293 the inlet, outlet temperature of tank and water temperature in the tank (K).

294 3.4 Performance of the system

295 The electrical efficiency of the PV/T panels is given by (Zhou et al., 2017):

$$296 \quad \eta_e = \frac{E_{pv}}{G A_{pvt}} \quad (18)$$

297 The thermal efficiency of the panels can be expressed as (Zhou et al., 2017):

$$298 \quad \eta_{t.th} = \frac{C_{p,wf} \dot{m}_{wf} (T_{th,o} - T_{th,i})}{G A_{th}} \quad (19)$$

299 Where A_{th} is the total effective area of thermal collector (m^2); $T_{th,i}$ and $T_{th,o}$ are
300 the temperatures at the inlet of the first thermal panel and the outlet of the last thermal
301 panel (K), respectively.

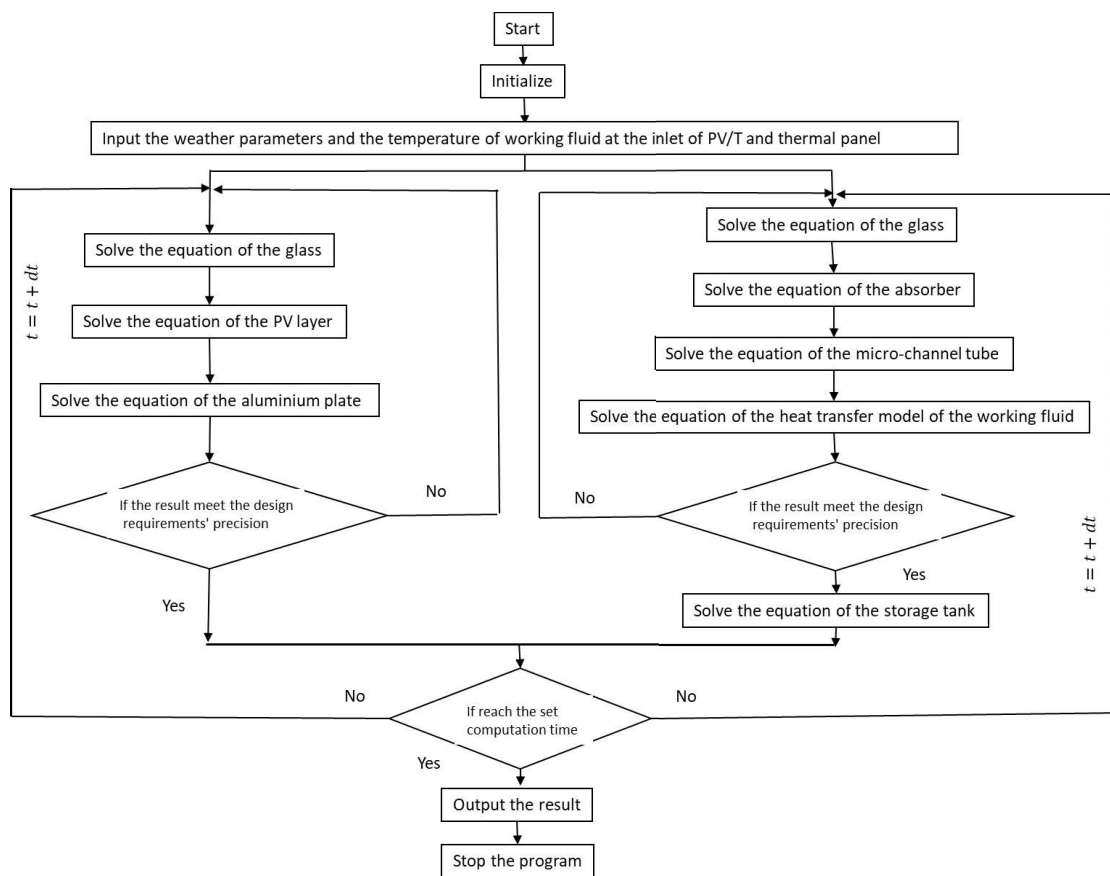
302 3.5 Model set-up and operational procedure

303 The equations of components of mini-channel PV/T panel, thermal collector and water
304 storage tank are developed. The iterative calculation of the above equations is solved
305 by the computer language C. The calculation flow chart is shown in **Fig. 10** and the

306 calculation steps are as follows:

- 307 1) Start the program, and initialize the parameters of the mini-channel PV/T and
308 thermal panel;
- 309 2) Input the weather parameters (solar radiation, ambient temperature, etc.), and
310 input the parameters at the inlet of the panels, including the temperature, mass
311 flow rate and specific enthalpy of the working fluid;
- 312 3) Solve the equation of the glass cover of PV/T panel, and calculate the
313 temperature of glass cover T_{gc} ;
- 314 4) Solve the equation of PV layer based on the glass cover temperature T_{gc} , and
315 calculate the temperature of the PV layer T_{pv} and output power of the PV/T
316 panel E_{pv} ;
- 317 5) Solve the equation of the aluminium plate based on the temperature of PV layer
318 T_{pv} and ambient temperature T_{am} , and calculate the temperature of absorber T_b ;
- 319 6) Solve the equation of the glass cover of thermal collector, and calculate the
320 temperature of glass cover T_{gc} ;
- 321 7) Solve the equation of the absorber and mini-channel tube of thermal collector,
322 and calculate its temperature T_b and T_p ;
- 323 8) Solve the equation of the working fluid; calculate the temperature at outlet of
324 thermal panel $T_{th,o}$;
- 325 9) Solve the equation of the storage tank, calculate the temperature of the water
326 T_w ;

- 327 10) Solve the equation of the working fluid; calculate the temperature at outlet of
 328 tank $T_{tk.o}$;
- 329 11) Check if the calculated value of each parameter has reached the calculation
 330 accuracy ($|T_{sim} - T_{set}|/T_{set} < 10^{-3}$, computation time 480 minutes) If no,
 331 return to step 3) and continue iterative solution; if yes, then output the results;
- 332 12) End the calculation program.



333

334 **Fig. 10 Calculation flow chart of mini-channel PV/T and thermal collector**
 335 **hot water system**

336 **4 Experimental performance of the system in summer**

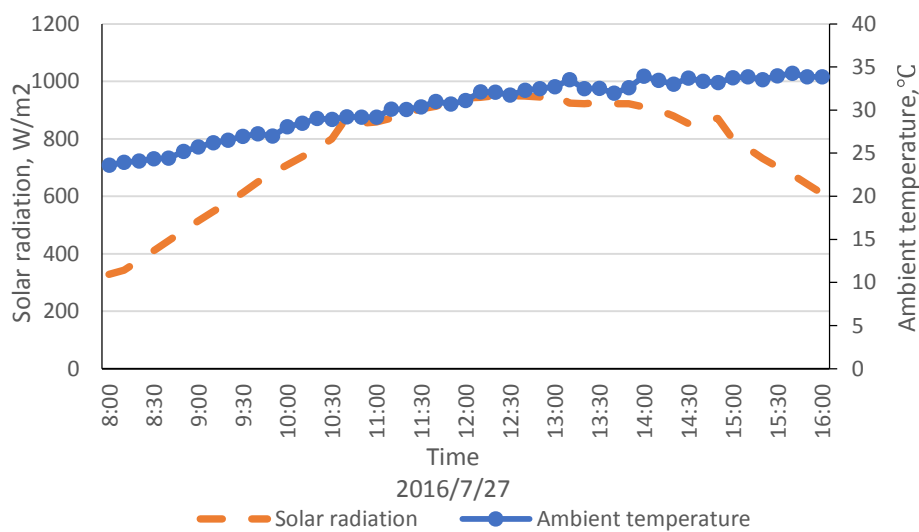
337 The performances of this system in winter under the clear days and low solar radiation

338 condition have been tested (Zhou et al., 2017; Zhou et al., 2020). In this paper, the
 339 performance of this system for generating hot water in summer is presented. The
 340 experiment is carried out from 21th to 27th July 2016. The testing result is shown in
 341 **Table 3**, and a typical day's weather data is chosen as the input parameters to verify the
 342 simulation model. The experimental and simulated results are compared.

343 **Table 3 Testing result of the system in summer**

Date	Radiation(W/m ²)	Temperature °C			System performance (%)	
		T_a	T_{wt}^i	T_{wt}^f	$\eta_{t.Th}$	$\eta_{e.PVT}$
21/07	685.6	13.2	22.2	56.1	45.6	11.9
22/07	703.4	12.8	22.7	57.4	46.2	11.5
23/07	697.5	11.1	23.1	56.9	45.8	11.8
24/07	736.4	9.1	22.9	57.8	44.9	12.0
25/07	743.8	8.4	22.5	58.6	47.0	11.0
26/07	723.6	8.7	21.6	56.9	46.3	11.2
27/07	765.5	6.4	23.2	59.3	46.8	11.5

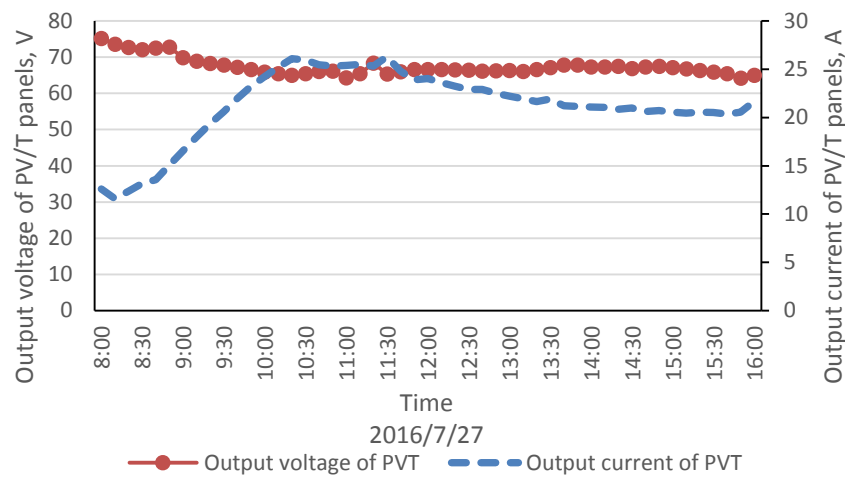
344



345

346 **Fig. 11 Variation of the solar radiation and ambient temperature in a sunny day**

347 **Fig. 11** displays the solar radiation and ambient temperature. The ambient temperature
348 increases with time and reaches a stable value at noon (from 23.5 °C to 33.5 °C during
349 8:00 to 13:10), and then keeps steady (33.8 °C) in the afternoon. The variation trend of
350 the solar radiation is a parabolic curve, which increases from 330 W/m² to 950 W/m²
351 (8:00 - 12:40), and then drops to 610 W/m² (12:40 - 16:00).



352

353 **Fig. 12 Output voltage and current of the PV/T panels in sunny day**

354 **Fig. 12** shows the output voltage and current of the PV/T panels. The output voltage of
355 the PV/T panel remains at 68 V, while the output current increased from 11.5 A to 26
356 A, and then dropped to 20 A during the testing time. The output current was not only
357 impacted by the solar radiation, but also the inverter. The inverter can show a good
358 performance when the voltage of battery is between 46 V to 52 V. However, the power
359 of the electrical load was stable, while the input power is changing all times, therefore,
360 the output current does not match the solar radiation very well sometimes.

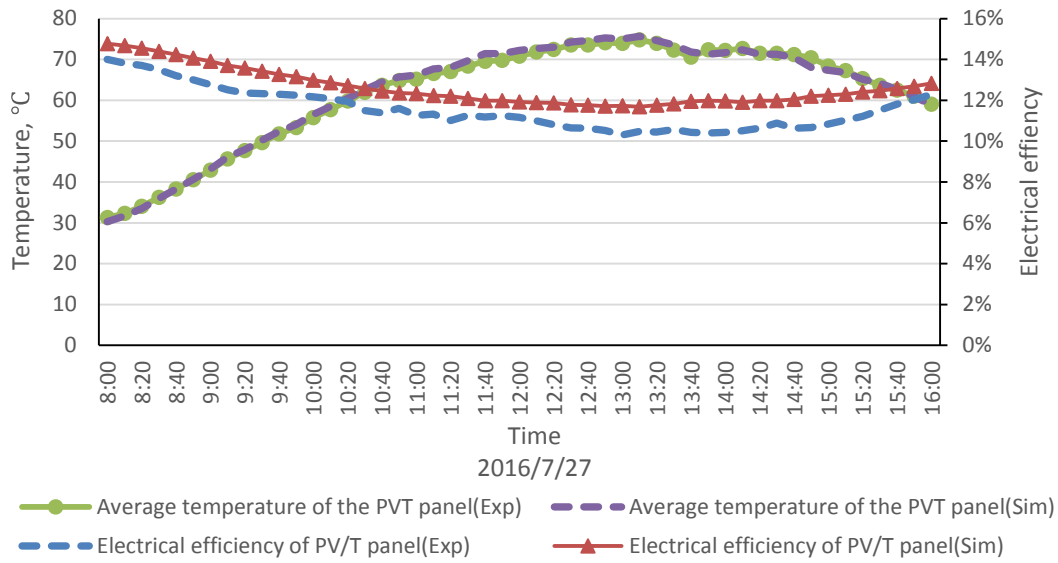
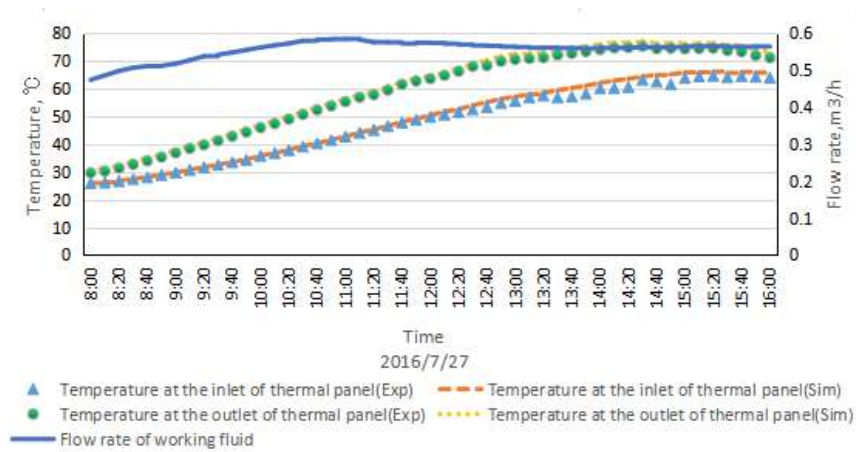


Fig. 13 Experimental and simulated absorber temperature and electrical efficiency of PV/T panels

Fig. 13 shows the variation of experimental and simulated absorber temperature and electrical efficiency of PV/T panels. With a natural convection cooling by the surrounding air, the surface temperature of PV/T panel is affected by the solar radiation. It shows a similar trend as solar radiation, which rises from 30 °C to 75 °C in the morning and then drops to 59 °C in the afternoon. The electrical efficiency shows an opposite trend as the solar radiation, because it is affected by the operating temperature, a high operating temperature with a lower electrical efficiency. The electrical efficiency ranges from 10.4% to 14.7%, and the average experimental and simulated electrical efficiency are 11.5% and 12.6%, respectively.

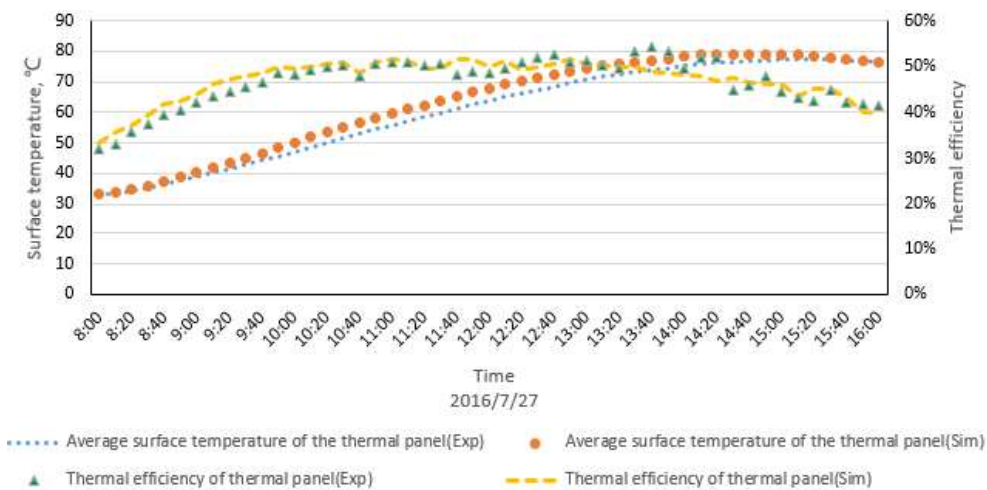
Fig. 14 shows the experimental and simulated inlet and outlet temperature of thermal collectors. These two temperatures are not only affected by the solar radiation but also by the water temperature in storage tank (Fig. 16). With the increase of water

376 temperature in the tank, the inlet temperature increases from 26 °C to 64 °C, while the
 377 outlet temperature increases from 30 °C to 77 °C and then drops to 71 °C. The
 378 temperature difference between the inlet and outlet ranges from 3 °C to 15 °C, and it
 379 increases from 8:00 to 13:00, then decreases in the afternoon. The flow rate of working
 380 fluid remains at 0.56 m³/h.



381

382 **Fig. 14 Experimental and simulated inlet, outlet temperature of thermal collector**
 383 **and flow rate of working fluid in it**

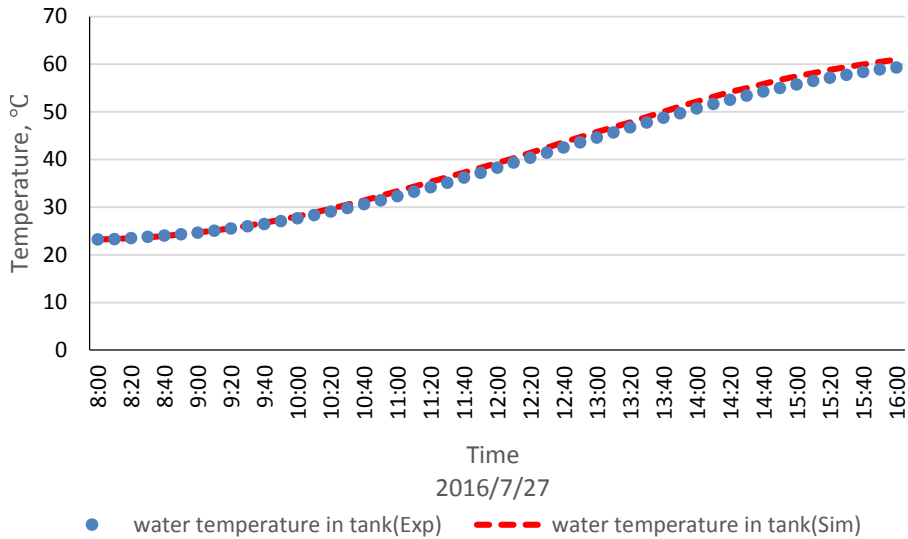


384

385 **Fig. 15 Experimental and simulated absorber temperature and thermal**
 386 **efficiency of thermal collector**

387 Similarly, the absorber temperature of thermal collectors (**Fig. 15**) is affected by the
388 solar radiation and inlet temperature of working fluid, and it shows a similar variation
389 trend as the inlet and outlet temperature of thermal collectors. It increases from 33 °C
390 to 79 °C and then decreases to 76 °C. The thermal efficiency is affected by the solar
391 radiation and temperature difference between the inlet and outlet of thermal panel, and
392 has a similar variation trend as them. It rises from 31.9% to 51.2% in the morning and
393 then drops to 41.4% in the afternoon. The thermal efficiency ranges from 33.5% to
394 51.6%, and the experimental and simulated daily average thermal efficiency are 46.8%
395 and 47.0%, respectively.

396 **Fig. 16** shows the variation of experimental and simulated water temperature in storage
397 tank. With the hot working fluid releasing thermal energy to the water continually, the
398 water temperature rises from 23 °C to 59 °C. The temperature variation speed is affected
399 by the solar radiation and thermal efficiency. When the solar radiation is not strong
400 (below 600 W/m²) and a low thermal efficiency, the water temperature rises very slowly
401 (4 °C in 2 hours), while when the solar radiation is high (over 600 W/m²) and high
402 thermal efficiency, it rises very quickly (32 °C in 6 hours).



403

404 **Fig. 16 Experimental and simulated water temperature in storage tank**

405 **4.1 Simulated VS experimental data analysis**

406 It can be found that most of the most significant results agreed with each other very
 407 well, and their error are shown in the **Table 4**. The high error of the performance
 408 efficiency is caused by several reasons, i.e., testing error, unstable practical operating
 409 condition. The electrical efficiency is impacted by the inverter and load, and the other
 410 efficiency is calculation value and affected by the measurement errors.

411 **Table 4 Average error of the system and performance**

	PVT		Thermal collector				Tank
	T_b (°C)	η_e	T_b (°C)	$T_{th.i}$ (°C)	$T_{th.o}$ (°C)	η_{th}	T_w (°C)
Experimental result	61.7	12.6%	60.4	47.7	58.9	46.8%	59.3
Simulated result	62.0	11.5%	62.9	48.7	60.4	47.0%	60.9
Error	5%	9.3%	4.2%	2.0%	2.4%	5.4%	2.7%

412

413 **5 Conclusion**

414 In this paper, a mini-channel PV/T and thermal collector hot water system is presented.

415 The novel PV/T panel and thermal collector use mini-channel tube as the heat
416 exchanger, which has a small hydraulic diameter and large heat exchanger area, to
417 enhance the heat transfer coefficient of working fluid, resulting in a higher electrical
418 and thermal efficiency. This system is designed, constructed and tested at the selected
419 clear days of Lvliang city, China.

420 The testing for generating hot water in summer is carried out, and an integral simulation
421 model is developed. One typical day's weather data is selected as the input parameters
422 to verify the simulation model. The experimental and simulated electrical efficiency of
423 PV/T panels are 11.5% and 12.6%, respectively. The inlet temperature of thermal panel
424 is related to the water temperature in the tank, and it increases first and remains steady.
425 The outlet temperature and surface temperature are affected by the inlet temperature
426 and solar radiation, and they show a rising trend first and a light decrease. The
427 experimental and simulated thermal efficiency of thermal collectors are 46.8% and
428 48.0%, respectively. The experimental and simulated final water temperatures in the
429 tank are 59.3 °C and 60.9 °C, respectively. The errors of these data are analyzed, and
430 the electrical efficiency has the maximum value of 9.3%, while inlet temperature of
431 thermal collector has the minimum value of 2.0%.

432 The experimental and simulation results of the system in summer provided fundamental
433 data and method for the performance analysis of whole year and improvement of similar

434 system in the future.

435 **Acknowledgement**

436 The work of this paper was sponsored by Shanxijingxu renewable energy Co. Ltd,
437 China.

438 **Reference**

439 A. Allouhi, M. Benzakour Amine, M.S. Buker, T. Kousksou, A. Jamil. Forced-
440 circulation solar water heating system using heat pipe-flat plate collectors: Energy
441 and exergy analysis. *Energy* 180 (2019) 429-443.

442 Aminreza Noghrehabadi, Ebrahim Hajidavalloo, Mojtaba Moravej. Experimental
443 investigation of efficiency of square flat-plate solar collector using SiO₂/water
444 nanofluid. *Case Studies in Thermal Engineering* 8 (2016) 378-386.

445 Ataollah Khanlari, Hande Özge Güler, Azim Dogus Tuncer, Ceylin Sirin, Yasar Can
446 Bilge, Yusuf Yılmaz, Afsin Güngör. Experimental and numerical study of the
447 effect of integrating plus shaped perforated baffles to solar air collector in drying
448 application. *Renewable Energy* 145 (2020) 1677-1692.

449 Bertoldi, P. Hirl, B. An econometric model to assess residential electricity savings in
450 the EU. In *Proceedings of the 7th International Conference EEDAL 2013 Energy
451 Efficiency in Domestic Appliances and Lighting*, Coimbra, Portugal, 11-13
452 September 2013.

453 China Building Energy Research Report (2018), China association of building energy
454 efficiency, Shanghai, 2018.11.12.

455 Davide Del Col, Andrea Padovan, Matteo Bortolato, Marco Dai Prè, Enrico Zambolin.
456 Thermal performance of flat plate solar collectors with sheet-and-tube and roll-
457 bond absorbers. *Energy* 58 (2013) 258-269.

458 Dongwei Zhang, Hanzhong Tao, Mimi Wang, Zishuai Sun, Chuan Jiang. Numerical
459 simulation investigation on thermal performance of heat pipe flat-plate solar
460 collector. *Applied Thermal Engineering* 118 (2017) 113-126.

461 F. Sarhaddi, S. Farahat, H. Ajam, A. Behzadmehr, M. Mahdavi Adeli. An improved
462 thermal and electrical model for a solar photovoltaic thermal (PV/T) air collector.
463 *Applied Energy* 87 (2010) 2328-2339.

464 H.A. Zondag, D.W. de Vries, W.G.J. van Helden, R.J.C. van Zolingen, A.A. van
465 Steenhoven. The yield of different combined PV-thermal collector designs. *Solar*
466 *Energy* 74 (2003) 253-269.

467 Jinzhi Zhou, Xudong Zhao, Xiaoli Ma, Zhongzhu Qiu, Jie Ji, Zhenyu Du, Min Yu.
468 Experimental investigation of a solar driven direct-expansion heat pump system
469 employing the novel PV/micro-channels-evaporator modules. *Applied Energy* 178
470 (2016) 484-495.

471 Jinzhi Zhou, Xudong Zhao, Xiaoli Ma, Yi Fan. Clear-days operational performance of
472 a hybrid experimental space heating system employing the novel mini-channel
473 solar thermal & PV/T panels and a heat pump. *Solar Energy* 155 (2017) 464-477.

474 Jinzhi Zhou, Xiaoli Ma, Xudong Zhao, Yanping Yuan, Min Yu, Jing Li. Numerical
475 simulation and experimental validation of a micro-channel PV/T modules based

476 direct-expansion solar heat pump system. *Renewable Energy* 145 (2020) 1992-
477 2004.

478 Jinzhi Zhou, Xudong Zhao, Yanping Yuan, Jing Li, Min Yu, Yi Fan. Operational
479 performance of a novel heat pump coupled with mini-channel PV/T and thermal
480 panel in low solar radiation, *Energy and Built Environment*,
481 <https://doi.org/10.1016/j.enbenv.2019.08.001>.

482 K. Balaji, S. Iniyan, V. Muthusamyswami. Experimental investigation on heat transfer
483 and pumping power of forced circulation flat plate solar collector using heat
484 transfer enhancer in absorber tube. *Applied Thermal Engineering* 112 (2017) 237-
485 247.

486 Khan JA, Monjur Morshed AKMM, Fang R. Towards ultra-compact high heat flux
487 micro-channel heat sink. *Procedia Eng* 90 (2014) 11-24.

488 Mahmoud Eltaweel, Ahmed A. Abdel-Rehim. Energy and exergy analysis of a
489 thermosiphon and forcedcirculation flat-plate solar collector using
490 MWCNT/Water Nanofluid. *Case Studies in Thermal Engineering* 14 (2019)
491 100416.

492 Mojtaba Edalatpour, Juan P. Solano. Thermal-hydraulic characteristics and exergy
493 performance in tube-on-sheet flat plate solar collectors: Effects of nanofluids and
494 mixed convection. *International Journal of Thermal Sciences* 118 (2017) 397-409.

495 Mohammad Sardarabadi, Mohammad Hosseinzadeh, Arash Kazemian, Mohammad
496 Passandideh-Fard. Experimental investigation of the effects of using metal-

497 oxides/water nanofluids on a photovoltaic thermal system (PVT) from energy and
498 exergy viewpoints. *Energy* 138 (2017) 682-695.

499 Pei Gang, Fu Huide, Zhang Tao, Ji Jie. A numerical and experimental study on a heat
500 pipe PV/T system. *Solar Energy* 85 (2011) 911-921.

501 Prajapati YK, Pathak M, Khan MK. Transient heat transfer characteristic of segmented
502 finned micro-channels. *Exp Therm Fluid Sci*, 79 (2016) 134-142.

503 R. Araya, F. Bustos, J. Contreras, A. Fuentes. Life-cycle savings for a flat-plate solar
504 water collector plant in Chile. *Renewable Energy* 112 (2017) 365-377.

505 R. Nasrin, N.A. Rahim, H. Fayaz, M. Hasanuzzaman, Water/MWCNT nanofluid based
506 cooling system of PVT: experimental and numerical research, *Renew. Energy* 121
507 (2018) 286-300.

508 Sandeep S. Joshi, Ashwinkumar S. Dhoble. Photovoltaic -Thermal systems (PVT):
509 Technology review and future trends. *Renewable and Sustainable Energy Reviews*
510 92 (2018) 848-882.

511 Sofia Tsemekidi Tzeiranaki, Paolo Bertoldi, Francesca Diluiso, Luca Castellazzi,
512 Marina Economidou, Nicola Labanca, Tiago Ribeiro Serrenho, Paolo Zangheri.
513 Analysis of the EU Residential Energy Consumption: Trends and Determinants.
514 *Energies* 2019, 12, 1065; doi:10.3390/en12061065.

515 Tisha Dixit, Indranil Ghosh. Review of micro-and mini-channel heat sinks and heat
516 exchangers for single phase fluids. *Renewable and Sustainable Energy Reviews*
517 41 (2015) 1298-1311.

518 Tolga Ural. Experimental performance assessment of a new flat-plate solar air collector
519 having textile fabric as absorber using energy and exergy analyses. *Energy* 188
520 (2019) 116116.

521 Tsemekidi-Tzeiranaki, S.; Bertoldi, P.; Labanca, N.; Castellezzi, L.; Serrenho, T.;
522 Economidou, M.; Zangheri, P. *Energy Consumption and Energy Efficiency Trends*
523 *in the EU-28 for the Period 2000-2016*; EUR 29473 EN; Publications Office of
524 the European Union: Luxembourg, 2018.

525 T. T. Chow, J. Ji, W. He. Photovoltaic-Thermal Collector System for Domestic
526 Application. *Journal of Solar Energy Engineering*, 129 (2007) 205-209.

527 T.T. Chow, W. He, J. Ji. Hybrid photovoltaic-thermosyphon water heating system for
528 residential application. *Solar Energy* 80 (2006) 298-306.

529 V.V. Tyagi, S.C. Kaushik, S.K. Tyagi. Advancement in solar photovoltaic/thermal
530 (PV/T) hybrid collector technology. *Renewable and Sustainable Energy Reviews*
531 16 (2012) 1383-1398.

532 W. Aziz, S.K. Chaturvedi, A. Kheireddine. Thermodynamic analysis of two-component,
533 two-phase flow in solar collectors with application to a direct-expansion solar-
534 assisted heat pump. *Energy* 24 (1999) 247-259.

535 Wei Pang, Qian Zhang, Yanan Cui, Linrui Zhang, Hongwen Yu, Xiaoyan Zhang,
536 Yongzhe Zhang, Hui Yan. Numerical simulation and experimental validation of a
537 photovoltaic/thermal system based on a roll-bond aluminum collector. *Energy* 187
538 (2019) 115990.

539 WORKING DOCUMENT Review of available information Accompanying the
540 document Communication from the Commission to the European Parliament, the
541 Council, the European Economic and Social Committee and the Committee of the
542 Regions on an EU Strategy for Heating and Cooling {COM(2016) 51 final}
543 https://ec.europa.eu/energy/sites/ener/files/documents/1_EN_autre_document_tra
544 [vail_service_part1_v6_0.pdf](https://ec.europa.eu/energy/sites/ener/files/documents/1_EN_autre_document_tra_vail_service_part1_v6_0.pdf)

545 Xiaolin Sun, Jingyi Wu, Yanjun Dai, Ruzhu Wang. Experimental study on roll-bond
546 collector/evaporator with optimized channel used in direct expansion solar assisted
547 heat pump water heating system. Applied Thermal Engineering 66 (2014) 571-
548 579.

549 Yogi Goswami D. Principles of solar engineering. Third ed. CRC Press Taylor & Francis
550 Group; 2015.

551 Zahra Hajabdollahi, Hassan Hajabdollahi. Thermo-economic modeling and multi-
552 objective optimization of solar water heater using flat plate collector. Solar Energy
553 155 (2017) 191-202.

554 Zheng Xinye, Ping Qin. 2014. "Characteristics of residential energy consumption in
555 China: Findings from a household survey." Energy Policy 75: 126-135.

556

557